A Unique Voltage Sensor Sensitizes the Potassium Channel AKT2 to Phosphoregulation

Erwan Michard,[1,2,3] Benoît Lacombe,[3] Fabien Porée,[1,2] Bernd Mueller-Roeber,[1,2] Hervé Sentenac,[3] Jean-Baptiste Thibaud,[3] and Ingo Dreyer[1,2,3]

[1]Universität Potsdam, Institut für Biochemie und Biologie, Abteilung Molekularbiologie, D-14476 Potsdam-Golm, Germany
[2]Max-Planck Institute of Molecular Plant Physiology, Cooperate Research Group, D-14424 Potsdam-Golm, Germany
[3]Laboratoire de Biochimie et Physiologie Moléculaire des Plantes, UMR 5004, Agro-M/CNRS/INRA/UM2, F-34000 Montpellier, France

Among all voltage-gated K^+ channels from the model plant *Arabidopsis thaliana*, the weakly rectifying K^+ channel (K_{weak} channel) AKT2 displays unique gating properties. AKT2 is exceptionally regulated by phosphorylation: when nonphosphorylated AKT2 behaves as an inward-rectifying potassium channel; phosphorylation of AKT2 abolishes inward rectification by shifting its activation threshold far positive (>200 mV) so that it closes only at voltages positive of +100 mV. In its phosphorylated form, AKT2 is thus locked in the open state in the entire physiological voltage range. To understand the molecular grounds of this unique gating behavior, we generated chimeras between AKT2 and the conventional inward-rectifying channel KAT1. The transfer of the pore from KAT1 to AKT2 altered the permeation properties of the channel. However, the gating properties were unaffected, suggesting that the pore region of AKT2 is not responsible for the unique K_{weak} gating. Instead, a lysine residue in S4, highly conserved among all K_{weak} channels but absent from other plant K^+ channels, was pinpointed in a site-directed mutagenesis approach. Substitution of the lysine by serine or aspartate abolished the "open-lock" characteristic and converted AKT2 into an inward-rectifying channel. Interestingly, phosphoregulation of the mutant AKT2-K197S appeared to be similar to that of the K_{in} channel KAT1: as suggested by mimicking the phosphorylated and dephosphorylated states, phosphorylation induced a shift of the activation threshold of AKT2-K197S by about +50 mV. We conclude that the lysine residue K197 sensitizes AKT2 to phosphoregulation. The phosphorylation-induced reduction of the activation energy in AKT2 is ~6 kT larger than in the K197S mutant. It is discussed that this hypersensitive response of AKT2 to phosphorylation equips a cell with the versatility to establish a potassium gradient and to make efficient use of it.

INTRODUCTION

Potassium is the predominant, inorganic ion of plant cells where it plays a major role as an osmoticum contributing to cellular hydrostatic (turgor) pressure, growth, and responses to the environment. The transport of potassium is accomplished by a variety of transport proteins (Véry and Sentenac, 2003; Amtmann et al., 2004). An important role is played by voltage-gated potassium channels of the so-called *Shaker* family (Pilot et al., 2003). *Shaker*-like plant potassium channels belong to the superfamily of voltage-gated K^+ channels (Yellen, 2002). A functional K^+ channel is a tetramer built up of four α subunits as indicated by coexpression studies (MacKinnon, 1991; Dreyer et al., 1997) and directly evidenced by the X-ray structure of a voltage-dependent *Shaker* K^+ channel (Long et al., 2005a). A single α-subunit shows a topology of six transmembrane domains (identified as S1–S6) flanked by cytosolic NH_2 and COOH termini, and a P (pore) loop and helix between S5 and S6 that contribute to the channel pore and ion selectivity filter. The voltage-sensing property of voltage-gated potassium channels is associated with the first four transmembrane domains and mainly with the S4 helix (Bezanilla, 2000; Männikkö et al., 2002; Latorre et al., 2003).

The family of plant voltage-gated potassium channels segregates into at least three functionally different subfamilies (Pilot et al., 2003): (1) hyperpolarization-activated, inward-rectifying K_{in} channels mediate potassium uptake, (2) depolarization-activated, outward-rectifying K_{out} channels mediate potassium release, and (3) weak-rectifying K_{weak} channels can mediate both potassium uptake and release. A model system for investigations of the properties of K_{weak} channels is the *Arabidopsis* K_{weak} channel AKT2 (Cao et al., 1995b; Ketchum and Slayman, 1996; Marten et al., 1999; Lacombe et al., 2000; Dreyer et al., 2001; Hoth et al., 2001; Chérel et al., 2002; Geiger et al., 2002; Michard et al., 2005). In literature this channel is also called AKT3 and AKT2/3. AKT3 refers to a truncated AKT2 protein lacking the first 15 amino acids. In order

to be consistent with the gene nomenclature (Cao et al., 1995b) we used in all cases the name AKT2 throughout this manuscript. AKT2 is predominantly expressed in the phloem and in guard cells and was proposed to fulfill different functions in these tissues. Among them is the control of the electrical membrane potential. Thereby, AKT2 may regulate sugar transport in the phloem and may play a role in electric cell signaling and membrane excitability. AKT2 was also proposed to be involved in the plant response to drought by adjusting potassium/sugar homeostasis (Marten et al., 1999; Lacombe et al., 2000; Deeken et al., 2002).

However, the results from recent biophysical approaches brought new aspects into the interpretation of the physiological function of AKT2-like channels and fueled the speculations on their diverse roles in the plant (Michard et al., 2005). Detailed electrophysiological analyses revealed an unexpected bimodal gating behavior of AKT2. It was particularly demonstrated that this channel, depending on its phosphorylation state, displays either the properties of a K_{in} channel or acts as a "potassium selective leak." Indeed, it was shown that the unique gating behavior of K_{weak} channels originates from the superimposition of two distinct gating modes (Dreyer et al., 2001): so-called gating mode#1 AKT2 channels activate at voltages more negative than -50 mV, whereas gating mode#2 channels are open in the entire physiological voltage interval (-250 mV to $+50$ mV). Interestingly, mode#2 channels are also voltage gated and close at nonphysiological voltages more positive than $+100$ mV, suggesting that the mechanistic difference between mode#1 and mode#2 channels is mainly a shifted activation threshold.

Further studies indicated that the setting of the gating mode is correlated with the phosphorylation status of the channel protein. One single channel can be converted from one mode into the other by phosphorylation/dephosphorylation events (Dreyer et al., 2001; Chérel et al., 2002; Michard et al., 2005). Two putative phosphorylation sites highly conserved among the K_{weak} subfamily and located in the S4–S5 linker and in the S6–COOH terminus linker of AKT2-like polypeptides (e.g., AKT2-S210 and AKT2-S329) were identified. When both serines in AKT2 were mutated to alanines, the mutant channel was inward rectifying and thus mimicked gating mode#1 channels, and when both serines were mutated to asparagines the mutant channel exhibited instantaneous currents only and thus mimicked gating mode#2 channels (Michard et al., 2005).

Phosphorylation appears to be a widely used process to regulate the activity of plant ion channels (Dreyer et al., 2004). For instance, biochemical approaches evidenced the phosphorylation of the K_{in} channel KAT1 in planta (Li et al., 1998; Mori et al., 2000). However, at the functional level the modulation of KAT1 activity (Berkowitz et al., 2000) and gating (Tang and Hoshi, 1999) by phosphorylation was far less pronounced (activation threshold shifted by around $+50$ mV) compared with the effects observed on AKT2 (activation threshold shifted by $>+200$ mV). Thus, although the concept of phosphoregulation allows to explain all our experimental observations on AKT2, so far it raises the following question. Which molecular peculiarities render the gating of K_{weak} channels highly sensitive to phosphorylation when compared with K_{in} channels?

In the present study we created chimeras between the K_{weak} channel AKT2 and the K_{in} channel KAT1. The results indicated that the regions upstream of the pore (from the NH_2 terminus to S4) contain sites crucial for weak rectification. We identified a K_{weak}-specific lysine residue in the voltage-sensing S4 helix that is essential for the weak rectification properties of AKT2. We conclude that the presence of this lysine residue strongly sensitizes AKT2 to phosphoregulation.

MATERIALS AND METHODS

Molecular Genetics
Standard molecular genetic methods were employed. Site-specific mutations were generated with the pAlter mutagenesis system (for details see online supplemental material, available at http://www.jgp.org/cgi/content/full/jgp.200509413/DC1). Mutants were verified by sequencing. For expression, the coding regions of the various channels were cloned into the mammalian expression vector pCI (Promega).

Expression and Electrophysiology
Culture and transfection of COS-7 cells as well as whole-cell and single channel recordings from COS cells were performed as described previously (Dreyer et al., 2001). The bath solution as well as the pipette solution in the cell-attached configuration contained (in mM) 150 KCl, 1 $CaCl_2$, 1.5 $MgCl_2$, 10 HEPES/NaOH (pH 7.4). The whole-cell pipette solution contained (in mM) 150 KCl, 1.5 $MgCl_2$, 3 EGTA, 10 HEPES/NaOH (pH 7.2), 2.5 MgATP. This ATP concentration had been shown to avoid channel activity rundown (Michard et al., 2005). Expression in *Xenopus* oocytes was performed as previously described (Dreyer et al., 2001). Measurements were repeated routinely at the end of each treatment with the addition of 10 mM Cs^+ to distinguish AKT2 currents and any background, nonselective leak, and to set a baseline of relative conductance. When 10 mM extracellular Cs^+ was applied, almost 100% of AKT2-mediated currents were blocked at voltages more negative than -150 mV (Lacombe et al., 2000).

Data Analyses
Data were analyzed according to common protocols (Sakmann and Neher, 1995; Blatt, 2004). Relative conductance (rel.G[V]) was obtained from tail current ($I_0[V]$) analyses with double-pulse voltage-clamp protocols in whole-cell recordings (Dreyer et al., 2001): after activating pulses in the -180 to $+140$ mV range, tail currents were recorded at voltage V_T (e.g., -40 mV). These tail currents displayed exponential deactivation kinetics. The instantaneous tail current (I_0) was obtained by extrapolating the kinetics to the time of the voltage jump to V_T and subsequently plotted against the voltage V applied during the preceding activating

pulse. $I_0(V)$ is proportional to the conductance (rel.G[V]) at the end of the activating pulse. For channels displaying two distinct gating modes (e.g., AKT2), a sum of two scaled Boltzmann functions was fitted to the resulting curves such that

$$I_0(V) = \frac{I_{max.mode\#1}}{1 + e^{-\delta_1 \frac{F}{RT}(V - V_{1/2,1})}} + \frac{I_{max.mode\#2}}{1 + e^{-\delta_2 \frac{F}{RT}(V - V_{1/2,2})}}, \quad (1)$$

where F, R, and T have their usual meaning, δ_1 and δ_2 denote the apparent gating charges, and $V_{1/2,1}$ and $V_{1/2,2}$ the half-activation voltages of the two modes. Because the $I_0(V)$ data in the experimentally accessible voltage interval from -180 to $+140$ mV were not sufficient to robustly fit all six free parameters independently, usually constraints were imposed on the parameters (details are outlined in the figure legends). Fittings were performed using a Marquardt-Levenberg algorithm (Marquardt, 1963) and the resulting values used to calculate relative conductance (rel.G) separately for the different gating modes:

$$rel.G_{mode\#1}(V) = \frac{I_0(V) - \dfrac{I_{max.mode\#2}}{1 + e^{-\delta_2 \frac{F}{RT}(V - V_{1/2,2})}}}{I_{max.mode\#1}} \quad (2)$$

$$rel.G_{mode\#2}(V) = \frac{I_0(V) - \dfrac{I_{max.mode\#1}}{1 + e^{-\delta_1 \frac{F}{RT}(V - V_{1/2,1})}}}{I_{max.mode\#2}}. \quad (3)$$

For AKT2 mutants displaying apparently only one gating mode Eq. 1 was applied with $I_{max.mode\#2} = \delta_2 = V_{1/2,2} = 0$. All results are reported as mean $\pm$ 1 SD where appropriate. To describe gating with a two state model and to quantify the energy difference between open and closed state, ΔG_{OC}, a Boltzmann function was fitted to the mean rel.G(V) values:

$$rel.G(V) = \frac{1}{1 + e^{-\left(\frac{\Delta G_{OC}}{kT}\right)}} = \frac{1}{1 + e^{-\delta \frac{F}{RT}(V - V_{1/2})}}, \quad (4)$$

resulting in $\Delta G_{OC} = \delta \times F/(RT) \times (V - V_{1/2}) \times kT$ values, which could be compared.

Single channel currents were low-pass filtered at 2.5 kHz and sampled at 10 kHz. Traces showing a stable baseline were used to generate histograms with bin width of 0.02 pA. Histograms were fitted with sums of Gauss functions:

$$histo(i_{bin}) = \sum_{k=0}^{N} \frac{A_k}{\sqrt{2\pi}\sigma_k} exp\left[-\frac{(i_{bin} - i_k)^2}{2\sigma_k^2}\right]. \quad (5)$$

Each Gauss function is characterized by a mean value i_k, a variance σ_k, and an amplitude A_k. $k = 0$ represents the channel in the closed conformation, $k = 1$ one open channel, $k = 2$ two open channels, etc. Single channel amplitudes were deduced from the differences between the means: $I_{SC} = i_1 - i_0$. The channel open probability was calculated from the relations between the surfaces under the different Gauss curves. If a patch contained only one active channel ($N = 1$) p_{open} was calculated as $p_{open} = A_1/(A_1 + A_0)$. One patch out of seven contained three channels. In this case the binomial distribution was applied, i.e., p_{open} was deduced from fitting to the following set of four equations:

$$A_3/(A_0 + A_1 + A_2 + A_3) = (p_{open})^3 \quad (6.1)$$

$$A_2/(A_0 + A_1 + A_2 + A_3) = 3 \cdot (p_{open})^2 \cdot (1 - p_{open}) \quad (6.2)$$
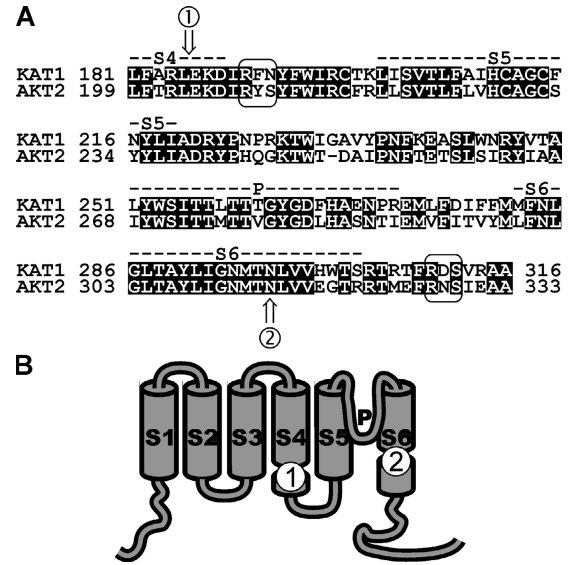

Figure 1. Sequence alignment to illustrate generation of chimeras. (A) Amino acid comparison of the S4–S6 regions of KAT1 and AKT2. The two pinpointed putative phosphoserines [RYS–210] and [RNS–329] together with the corresponding KAT1 motifs are labeled by boxes. The labels 1 (XhoI restriction site in the underlying plasmids) and 2 (BstXI restriction site in the underlying plasmids) indicate the sites used to swap domains. (B) Schematic representation of the topological location of the sites 1 and 2 in a channel subunit.

$$A_1/(A_0 + A_1 + A_2 + A_3) = 3 \cdot p_{open} \cdot (1 - p_{open})^2 \quad (6.3)$$

$$A_0/(A_0 + A_1 + A_2 + A_3) = (1 - p_{open})^3 \quad (6.4)$$

Online Supplemental Material

The online supplemental material (available at http://www.jgp.org/cgi/content/full/jgp.200509413/DC1) provides details on the cloning strategies and the primers used to generate mutants and chimeras.

RESULTS

The Region Upstream the S5 Segment Contains Elements Essential for Weak Rectification

Previous studies suggested that nonphosphorylated plant K_{weak} channels share functional similarities with K_{in} channels. After phosphorylation, however, their functional characteristics fundamentally diverge. Nonphosphorylated (mode#1) K_{weak} channels mediate time- and voltage-dependent inward potassium currents, whereas phosphorylated (mode#2) K_{weak} channels mediate instantaneous, leak-like potassium currents. Usually, in standard electrophysiological experiments, these two components superimpose and generate the impression of a weak rectification of the currents.

To understand the apparent differences in phosphoregulation between the K_{in} channel KAT1 and the K_{weak}
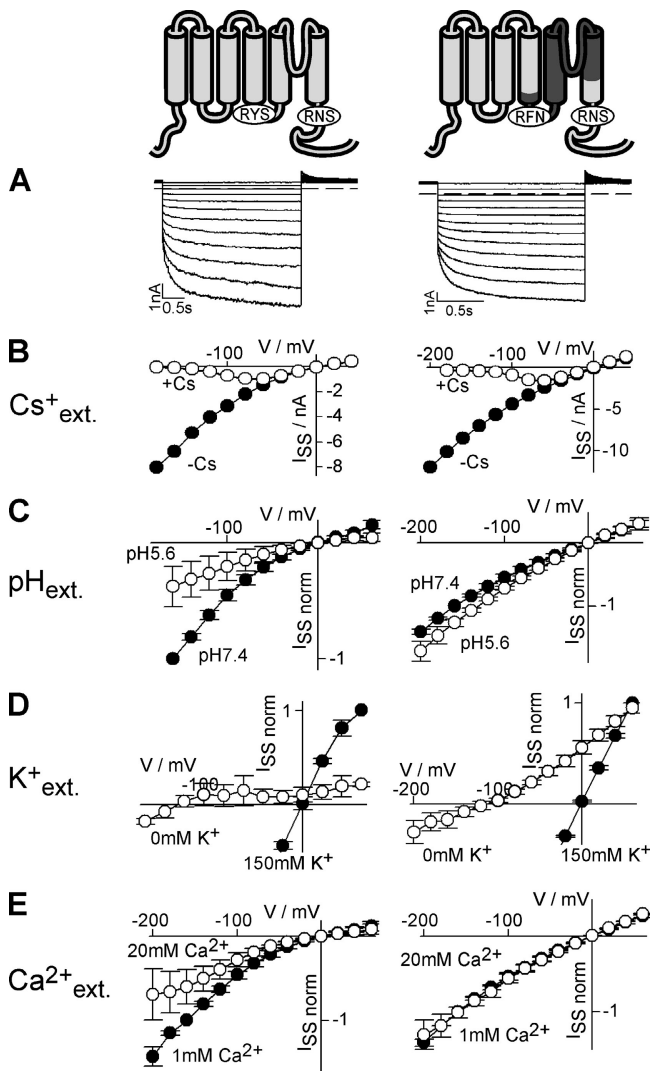
Figure 2. Exchange of the AKT2 pore by the KAT1 pore does not affect gating but alters the permeation properties of the chimeric channel. Characteristics of AKT2 (left) and the chimera AKT2-S5-P-S6-KAT1 (right) expressed in COS cells. In the chimera the fragment AKT2-E204_N314 was replaced by the fragment KAT1-E186_N297. (A) Currents elicited by voltage steps (AKT2: 3 s; chimera: 1.6 s) from a holding potential of +40 mV to voltages from +40 mV to −180 mV (20-mV decrements). The dashed lines indicate the zero current level. (B) Steady-state current–voltage characteristics. Currents were measured in standard solution (black circles) and after the addition of 10 mM Cs$^+$ to external standard solution (white circles). Data displayed in A and B are representative for at least three repeats. (C) Normalized current–voltage characteristics measured at pH 7.4 (black) and pH 5.6 (white). Currents were normalized to the current values measured at −160 mV at pH 7.4 (I$_{SS}$[−160 mV; pH 7.4] = −1). Data are displayed as mean ± SD (n = 3–8). (D) Normalized current–voltage characteristics measured in the presence (standard solution; black) and absence of external potassium (white; KCl in standard solution was replaced by NaCl). Currents were normalized to the current values measured at +60 mV in standard solution (I$_{SS}$[+60 mV; 150 mM K$^+$] = 1). Data are displayed as mean ± SD (n = 3). (E) Normalized current–voltage characteristics measured in bath solutions containing 1 mM Ca^{2+} (standard solution; black) and 20 mM Ca^{2+} (standard solution + 19 mM CaCl$_2$; white). Currents
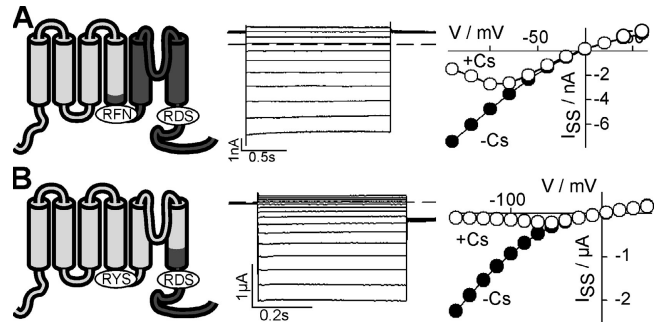

Figure 3. AKT2-KAT1 chimeras show "open-locked" behavior. Chimeras' structure (see also Fig. 1) is indicated (left). Parts originating from AKT2 are illustrated in light gray and parts from KAT1 in dark gray. Current traces (middle) and steady-state current–voltage characteristics (right) of the chimeras. Currents were measured in standard solution (black circles) and after the addition of 10 mM Cs$^+$ to external standard solution (white circles). The dashed lines indicate the zero current level. (A) Expression in COS cells. Currents elicited by 1.6-s voltage steps from a holding potential of +40 mV to voltages from +60 mV to −140 mV (20-mV decrements). (B) Expression in oocytes (100 mM KCl in the bath); 0.5-s voltage steps from 0 mV to voltages from +50 mV to −160 mV (15-mV decrements) followed by a step to −60 mV. Data displayed in A and B are representative for at least three repeats.

channel AKT2, we constructed recombinant chimeric channels between both. We swapped (a) the region between S4 and the COOH terminus comprising the P domain, (b) the COOH termini, and (c) the entire regions downstream the S4 segment (Figs. 1–4). The electrophysiological phenotypes of the chimeras were analyzed after expression in COS cells and *Xenopus* oocytes (Figs. 2–4). When the fragment between S4 and the COOH terminus of AKT2 was replaced by the corresponding region of KAT1, the chimera exhibited a voltage-dependent gating identical to the AKT2 wild-type characterized by the two K$^+$ current components: an instantaneous "leak-like" component and a hyperpolarization-activated time-dependent component (Fig. 2 A). The two current components of both channels were blocked by extracellular Cs$^+$ ions (Fig. 2 B). A more refined pharmacological fingerprint, however, unmasked the chimera. In contrast to wild-type AKT2, the chimera was neither blocked by protons (Fig. 2 C) nor sensitive to a reduction in the external K$^+$ concentration (Fig. 2 D). Additionally, the chimera was less Ca^{2+} sensitive when compared with AKT2 (Fig. 2 E). Consequently, with respect to its susceptibility toward

were normalized to the current values measured at −160 mV in 1 mM Ca^{2+} (I$_{SS}$[−160 mV; 1 mM Ca^{2+}] = −1). Data are displayed as mean ± SD (n = 3). It should be noted that, with respect to the permeation properties, the chimera behaved essentially like KAT1 (Hedrich et al., 1995; Véry et al., 1995; Becker et al., 1996; Hoth et al., 1997; Dreyer et al., 1998), the donor of the pore.
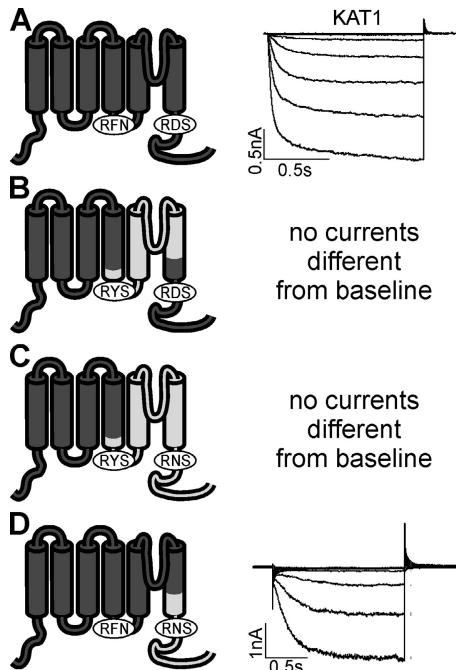
Figure 4. AKT2-KAT1 chimeras containing the NH₂ terminus and the first four membrane-spanning segments (S1–S4) of KAT1. (A) KAT1 mediates inward-rectifying currents. Currents were elicited in 1.2-s voltage steps from +40 mV to voltages between +40 mV and −160 mV (20-mV decrements). (B) No currents could be detected when the fragment KAT1-E186_N297 was replaced by the fragment AKT2-E204_N314. (C) No currents could be detected when the fragment KAT1-E186_N677 was replaced by the fragment AKT2-E204_I802. (D) The chimera KAT1-Ct$_{AKT2}$ mediates inward currents. The fragment KAT1-N297_N677 was replaced by the fragment AKT2-N314_I802. Currents were elicited in 1.6-s voltage steps from +60 mV to voltages between +60 mV and −200 mV (20-mV decrements). Data in A–D are representatives from at least three independent repeats each.

Figure 5. K$_{weak}$ channels contain an additional lysine residue in S4. Sequence comparison of the putative voltage-sensing segment of AKT2 (GenBank/EMBL/DDBJ accession no. AAA97865) with those of other plant K⁺ channels: the *Arabidopsis* K$_{out}$ channels SKOR (Q9M8S6) and GORK (Q94A76), the *Arabidopsis* K$_{in}$ channels KAT1 (AAA32824) and AKT1 (Q38998), and the (putative) K$_{weak}$ channels ZMK2 (CAB54856) from *Zea mays*, VFK1 (CAA71598) from *Vicia faba*, SPICK1 (AAD16278) and SPICK2 (AAD39492) from *Samanea saman*, SKT2 (CAA70870) from *Solanum tuberosum*, NpKT1 (BAA84085) from *Nicotiana paniculata*, NKT2 (BAD81033) from *Nicotiana tabacum*, PTK2 (CAC05489) from *Populus tremula x Populus tremuloides*, and OsKC (AAS90668) from *Oryza sativa*. Charged residues present in all channels are marked. Residues AKT2-G186 (see Fig. 6) and KAT1-S168 are displayed in bold letters. Additionally, the K$_{weak}$-specific lysine residue is highlighted.

H⁺, K⁺, and Ca²⁺, the chimera had the features of the KAT1 pore (Hedrich et al., 1995; Véry et al., 1995; Becker et al., 1996; Hoth et al., 1997; Dreyer et al., 1998) rather than the features of the AKT2 pore (Fig. 2, left; Hoth et al., 2001; Geiger et al., 2002). Thus, the replacement of the pore altered the properties of the permeation pathway. However, this exchange left the gating properties unaffected.

When the entire region downstream the S4 segment of AKT2 was replaced by that of KAT1, the resulting chimera mediated only instantaneously activating currents. A time-dependent component was not observable (Fig. 3 A). Similar results were obtained when only the COOH terminus was exchanged (Fig. 3 B), indicating that the COOH terminus of KAT1 is influencing the gating process differently compared with the AKT2 COOH terminus.

The inverse chimeras comprising the NH₂ terminus and the first four membrane-spanning segments (i.e., S1–S4) of KAT1 mediated either inward-rectifying cur-

rents or were electrically silent (Fig. 4). Interestingly, the exchange of the COOH termini did not alter the gating properties. The features of the chimera KAT1-Ct$_{AKT2}$ (Fig. 4 D) were not fundamentally different from that of the KAT1 wild type (Fig. 4 A).

Taken together, the results indicated that the putatively voltage-sensing module of AKT2, i.e., the NH₂ terminus and the first four membrane-spanning segments, confers the weak rectification property on the chimeric channels (for comparison see Cao et al., 1995a). In the following we investigated further the role of the putative primary voltage sensor, the S4 segment, in AKT2 channel gating.

The S4 Segment Is Involved in AKT2 Gating

Voltage-dependent gating of diverse animal and plant voltage-gated channels has been shown to depend on the S4 segment carrying a high density of positive charges (Dreyer et al., 1999, 2004; Männikkö et al., 2002; Bezanilla and Perozo, 2003; Latorre et al., 2003; Swartz, 2004). Therefore, this region was proposed to be also involved in the gating of plant K$_{weak}$ channels (Michard et al., 2005). To elucidate the role of the S4 segment (ranging from AKT2-L285 to AKT2-D206; Fig. 5) in AKT2 gating, we introduced an additional charge at position G186 by generating the mutation AKT2-G186R. The mutation did not alter the bimodal gating feature of the AKT2 channel (Fig. 6, A–C). Like the
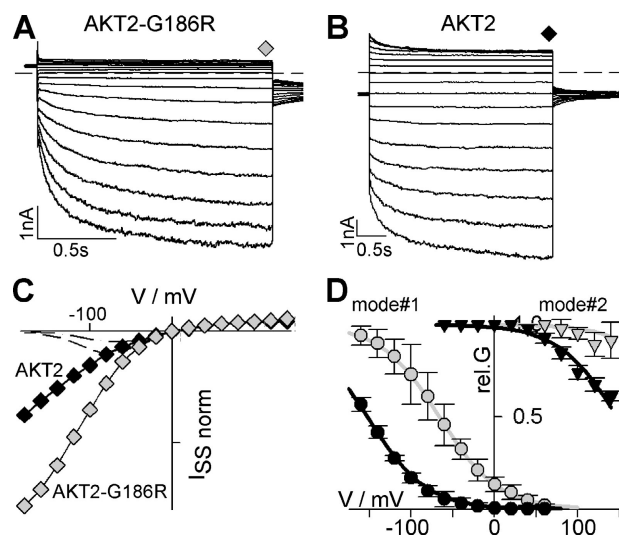
Figure 6. Mutation in S4 affects gating of AKT2. (A) Representative K^+ currents obtained from one COS cell expressing the mutant AKT2-G186R. Currents elicited by 1.6-s voltage steps from a holding potential of $+40$ mV to voltages from $+140$ mV to -180 mV (20-mV decrements) followed by a further voltage step to -40 mV (dashed line, zero-current level). (B) Representative K^+ currents obtained from one COS cell expressing the AKT2 wild type. Currents elicited by 3-s voltage steps from a holding potential of -40 mV to voltages from $+140$ mV to -180 mV (20-mV decrements; dashed line, zero-current level). (C) Normalized steady-state currents measured at the end of the voltage steps shown in A (AKT2-G186R, gray diamonds) and B (AKT2, black diamonds). To compare currents with a similar instantaneous component, currents were normalized to the amplitudes measured at $+60$ mV. Current amplitudes measured in the presence of 10 mM Cs^+ are indicated (AKT2, dash-dotted line; AKT2-G186R, dashed line). (D) Relative conductance of AKT2 (black symbols) and AKT2-G186R (gray symbols) separated for gating mode#1 (circles) and #2 (triangles). Data are displayed as mean $\pm$ SD ($n = 4$–5). Solid lines represent nonlinear least-squares fittings of Eq. 4 to the data. To reduce the number of free parameters, fits were constrained by the following: (a) only one δ value was adjusted for all four datasets, and (b) the difference in the $V_{1/2}$ values between the two modes was kept identical in the wild type and in the mutant. The fit yielded $\delta = 0.71$, $V_{1/2}^{AKT2\text{-}mode\#1} = -152.3$ mV, $V_{1/2}^{AKT2\text{-}mode\#2} = +147.1$ mV, $V_{1/2}^{AKT2\text{-}G186R\text{-}mode\#1} = -65.9$ mV, $V_{1/2}^{AKT2\text{-}G186R\text{-}mode\#2} = +233.5$ mV.

AKT2 wild type, the mutant AKT2-G186R mediated both an instantaneous current component and a hyperpolarization-activated time-dependent current component (Fig. 6, A and B). However, the gating properties of the mutant channel were affected (Fig. 6 D): an analysis of the deactivation currents ("tail current" analysis as described in MATERIALS AND METHODS and in Dreyer et al., 2001) revealed a strong shift of the voltage dependence of channels of both gating modes. For the gating mode#1 (nonphosphorylated state; AKT2 wild-type channels function as inward rectifiers) the shift could be quantified to be $\sim+85$ mV (Fig. 6 D). Interestingly, the generation of an additional positive charge in the S4 segment of the K_{weak} channel AKT2

had a similar effect as previously shown for the K_{in} channel KAT1. In KAT1 the equivalent mutation, KAT1-S168R, changed the properties of voltage sensing by inducing a shift of the channel activation threshold by about $+100$ mV (Dreyer et al., 1997). The S4 segment may therefore be involved in the gating of AKT2 mode#1 channels as it has been shown for hyperpolarization-activated channels from plants (Latorre et al., 2003) and animals (Männikkö et al., 2002). In addition, the results indicated that the S4 segment was also involved in the unusual gating of AKT2 mode#2 (phosphorylated state) channels. Like in gating mode#1, also in gating mode#2 the mutant AKT2-G186R activated at more positive voltages than the wild type. The data were well described if we assumed that the mutation induced an identical shift in both gating modes (Fig. 6 D, gray lines).

A Lysine Residue in S4 Is Essential for the Instantaneous Current Component of AKT2

We identified nine channels closely related to AKT2 in publicly available databases, showing 60–75% identity with AKT2 and constituting a distinct channel subfamily (K_{weak} channels) (Pilot et al., 2003). These channels exhibit the conserved putative phosphorylation sites in the S4–S5 linker and downstream of the S6 segment, which were shown to be involved in setting the gating mode of AKT2 (Michard et al., 2005). The S4 segments of channels from the AKT2 subfamily were compared with those of K_{in} and K_{out} channels (Fig. 5). Among the different channel subfamilies, six positively charged residues (R or K) are highly conserved (Fig. 5, "+"). Positive residues in S4 are assumed to be essential for the task of voltage sensing (Bezanilla and Perozo, 2003; Swartz, 2004). In addition to these conserved charged residues, the S4 segment of AKT2 comprises two further positive charges: a lysine residue at AKT2-K197 (Fig. 5, arrow) and a histidine residue at AKT2-H198. Notably, the lysine residue is conserved in all members of the K_{weak} subfamily. K_{in} and K_{out} channels possess noncharged residues at the equivalent positions. The sequence comparison further revealed that the S4 segments of K_{weak}, K_{in}, and K_{out} channels show at the targeted positions the largest diversity.

Both, K197 and H198 were mutated to serines (Fig. 7), residues found at the equivalent positions in KAT1, the K_{in} model channel. The mutation H198S did not markedly affect AKT2 gating (Fig. 7 B). In contrast, the single mutant AKT2-K197S as well as the double mutant AKT2-K197S-H198S resembled plant K_{in} channels, i.e., they were purely inward rectifying (Fig. 7, A and C). Both mutants completely lacked the instantaneous current component and only exhibited time- and voltage-dependent currents upon voltage stimulation more negative than -80 mV. A similar result was obtained
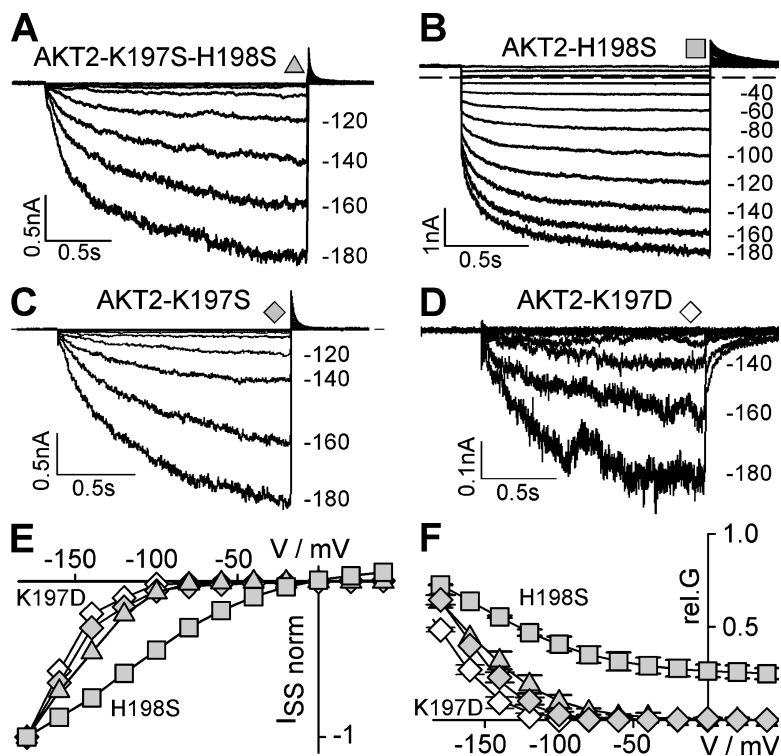
Figure 7. An exceptional lysine residue in the S4 segment is unique to K_{weak} channels and is essential for weak rectification. (A–D) Replacement of the histidine in S4 by serine does not change gating; replacement of the neighbored lysine abolishes "open leak" behavior. Representative K^+ currents obtained from COS cells expressing (A) AKT2-K197S-H198S, (B) AKT2-H198S, (C) AKT2-K197S, and (D) AKT2-K197D. Currents were elicited in voltage steps from +40 mV to voltages from +40 mV to −180 mV (20-mV decrements; dashed line, zero-current level). (E) Steady-state current–voltage characteristics measured at the end of the activation voltage steps shown in A–D (AKT2-K197S-H198S, gray triangles; AKT2-H198S, gray squares; AKT2-K197S, gray diamonds; AKT2-K197D, white diamonds). Currents were normalized to the current values measured at −180 mV (I_{SS}[−180 mV] = −1). (F) Relative conductance of AKT2-K197S-H198S (gray triangles), AKT2-H198S (gray squares), AKT2-K197S (gray diamonds), and AKT2-K197D (white diamonds). Data are displayed as mean ± SD (n = 3–6). Solid lines represent nonlinear least-squares fittings of Eqs. 1 and 4 to the data yielding δ = 1.37, $V_{1/2}^{AKT2-K197S}$ = −160.7 mV, $V_{1/2}^{AKT2-K197D}$ = −175.5 mV, $V_{1/2}^{AKT2-K197S-H198S}$ = −161.8 mV, and $I_{max.mode\#2}^{AKT2-H198S}$ = 0.24, $I_{max.mode\#1}^{AKT2-H198S}$ = 0.76, $\delta_1^{AKT2-H198S}$ = 0.59, $V_{1/2,1}^{AKT2-H198S}$ = −156.2 mV.

when the lysine at position AKT2-K197 was replaced by aspartate, a negatively charged amino acid. Like AKT2-K197S, the mutant AKT2-K197D was also inward rectifying (Fig. 7, D–F). For AKT2-K197D K^+ currents were observed only at voltages more negative than −120 mV, indicating that this mutant channel activated more negative than AKT2-K197S. Thus, the lysine residue in the S4 segment of AKT2 is essential for the presence of the instantaneous K^+ current component. Moreover, the charge born by the residue at position 197 appeared to be important in determining channel properties. Its neutralization (via the K197 to S mutation) abolished instantaneous currents, and its replacement by a negative charge (via the K197 to D mutation) had an even stronger effect, by additionally shifting the activation threshold to more negative voltages.

The similarity between AKT2-K197S and K_{in} channels was further evidenced at the single channel level. When we employed the patch-clamp technique on AKT2-K197S expressing COS cells in the inside-out configuration, AKT2-K197S activity was lost in the time range of seconds (even with 2.5 mM MgATP in the bath solution; unpublished data). We therefore performed AKT2-K197S single channel recordings in the cell-attached configuration (Fig. 8). When a membrane patch containing a single ion channel was challenged with different membrane voltages, channel openings were only observed at membrane voltages more negative than −80 mV. Frequency of channel openings and lifetime of the open state increased upon further mem-

brane hyperpolarization (Fig. 8 A). When the membrane voltage was stepped from −40 to −180 mV, channel activity was observed after a significant delay (Fig. 8 B, white arrow). After stepping back to −40 mV, the activated open channel remained open for a short time before it closed permanently (Fig. 8 B, gray arrow). The single channel conductance of the observed channel was ∼21 pS (Fig. 8 C), similar to that reported for the AKT2 wild type (25–30 pS) (Marten et al., 1999; Lacombe et al., 2000). Thus, the mutation K197S did not significantly alter the single channel conductance. Further evidence that the mutant AKT2-K197S underlies the investigated single channel activity was provided by analyzing the single channel open probability (Fig. 8 D). The single channel p_{open} values superimposed satisfyingly with the relative conductance values obtained for AKT2-K197S in whole-cell measurements (Fig. 8 D, solid line; Fig. 7 F). Thus, the gating features of the mutant AKT2-K197S resembled those of plant *Shaker*-like K_{in} channels (Hoshi, 1995; Mueller-Roeber et al., 1995; Zei and Aldrich, 1998).

The Response of AKT2-K197S to Phosphorylation Is Far Weaker than in the Wild Type

When expressed in COS cells or in *Xenopus* oocytes, the switch between the two gating modes of the AKT2 wild type is promoted by cell-intrinsic PKA-specific phosphorylation (Michard et al., 2005). The application of the PKA inhibitor H89 on AKT2-expressing oocytes induced an increase in time-dependent mode#1 currents
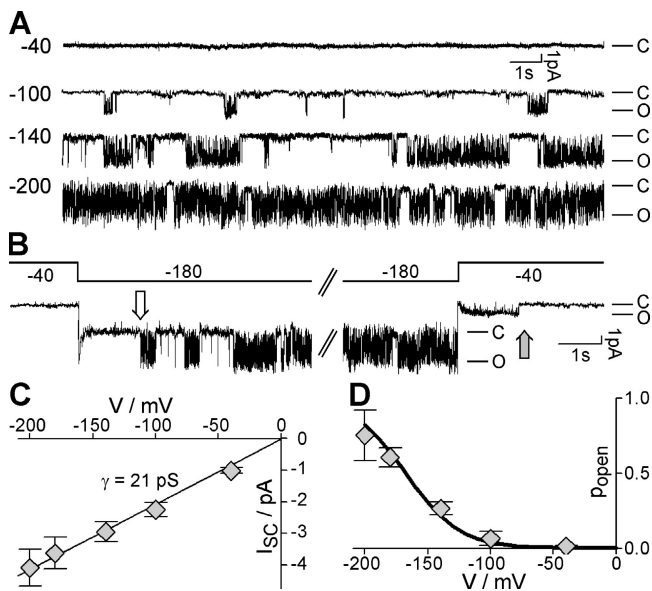
Figure 8. Single channel behavior of AKT2-K197S expressed in COS cells. (A) Representative single-channel currents (cell-attached) recorded at -40 mV, -100 mV, -140 mV, and -200 mV. C, closed state; O, open channel. (B) Delayed single channel activation and deactivation following voltage steps. Membrane voltage was stepped from -40 mV to -180 mV (left) and back to -40 mV (right). The voltage protocol is indicated. The white arrow illustrates the delayed activation at -180 mV; the gray arrow the delayed deactivation at -40 mV. (C) Current–voltage curve of the open K197S channel. Data are displayed as mean $\pm$ SD ($n =$ 3–4). Linear regression ($R^2 \approx 0.99$) resulted in a single channel conductance of $\gamma \approx 21$ pS (solid line). (D) Voltage-dependent open probability of single K197S channels. Data are displayed as mean $\pm$ SD ($n =$ 3–4). Solid line indicates the relative conductance of K197S deduced from macroscopic whole cell currents (from Fig. 7 F).

and a decrease in instantaneous mode#2 currents. The PKA activator Br-cAMP on the contrary increased mode#2 currents and decreased mode#1 currents. To investigate the role of phosphoregulation on the mutant AKT2-K197S we applied PKA inhibitors and activators to AKT2-K197S expressing *Xenopus* oocytes (Br-cAMP and H89) and COS cells (Br-cAMP), in parallel with experiments performed on the AKT2 wild type (Michard et al., 2005). However, whereas the effectors influenced the features of the wild type, the gating properties of AKT2-K197S were not significantly altered (unpublished data). Therefore we chose another approach to estimate the response of the K197S mutant to phosphorylation. As shown previously, the two double mutants AKT2-S210A-S329A (Fig. 9 B) and AKT2-S210N-S329N (Fig. 9 C) mimicked the dephosphorylated (mode#1) and the phosphorylated (mode#2) state of the AKT2 wild type, respectively (Fig. 9 G) (Michard et al., 2005). The AKT2-S210A-S329A mutant displayed inward-rectifying time-dependent currents, only, whereas the AKT2-S210N-S329N showed only instanta-

neous currents. Consequently, these double mutants were generated in the AKT2-K197S background (Fig. 9 D). Both triple mutants, AKT2-K197S-S210A-S329A (Fig. 9 E) and AKT2-K197S-S210N-S329N (Fig. 9 F), conducted inward-rectifying potassium currents when expressed in COS cells. Nevertheless, the two mutants differed in their activation threshold. Whereas AKT2-K197S-S210N-S329N was active at voltages more negative than -70 mV, AKT2-K197S-S210A-S329A activity was only observed at voltages more negative than -120 mV (Fig. 9 H).

The analysis of the gating properties of the triple mutants suggested that the AKT2-K197S mutant is still modulated by phosphorylation of the residues S210 and S329, but also that the phosphorylation of these two sites, instead of inducing a >200 mV shift of the activation potential (as observed for the AKT2 wild-type channel) only induced an ~ 50 mV shift in the AKT2-K197S mutant channel.

Quantification of the Role of K197 in Phosphoregulation of AKT2

To quantify the gating parameters of gating modes#1 and #2 of the AKT2 wild type and the channel AKT2-K197S, the gating of each of the four mutants S210A-S329A, S210N-S329N, K197S-S210A-S329A, and K197S-S210N-S329N was approximated by a two-state model in which a channel can either be open, O, or closed, C (Fig. 10 A). In this model, the relative conductance of each channel can be described by a Boltzmann function (Eq. 4, rel.G $= (1 + \exp[\Delta G_{OC}/kT])^{-1}$; Fig. 9 G and H, circles and triangles, gray lines). The relative conductance of the AKT2 wild type and the mutant K197S were well described by weighted sums of the Boltzmann functions obtained for the matching double A and double N mutants (Fig. 9, G and H, diamonds, black lines).

From the obtained parameters we could estimate in as much phosphorylation influenced the activation energies of the channels AKT2 and AKT2-K197S, assuming that the double A and double N mutants represent the dephosphorylated (mode#1) and phosphorylated state (mode#2) (Fig. 10 B). It turned out that for the AKT2 wild type, phosphorylation (inducing a transition from gating mode#1 to mode#2) reduced the energy needed to activate the channel by about $\Delta(\Delta G) \approx 9$ kT. As a consequence, the channel did not close and was locked in an open state in the entire physiological voltage range when phosphorylated. In contrast, the phosphorylation of the mutant AKT2-K197S resulted in a reduction of the activation energy of only $\Delta(\Delta G) \approx 2.3$ kT; ~ 6 kT smaller than in the wild type. As a consequence, changes of the phosphorylation status of the mutant do not dramatically affect channel gating, and the mutant AKT2-K197S appears to be similar to plant
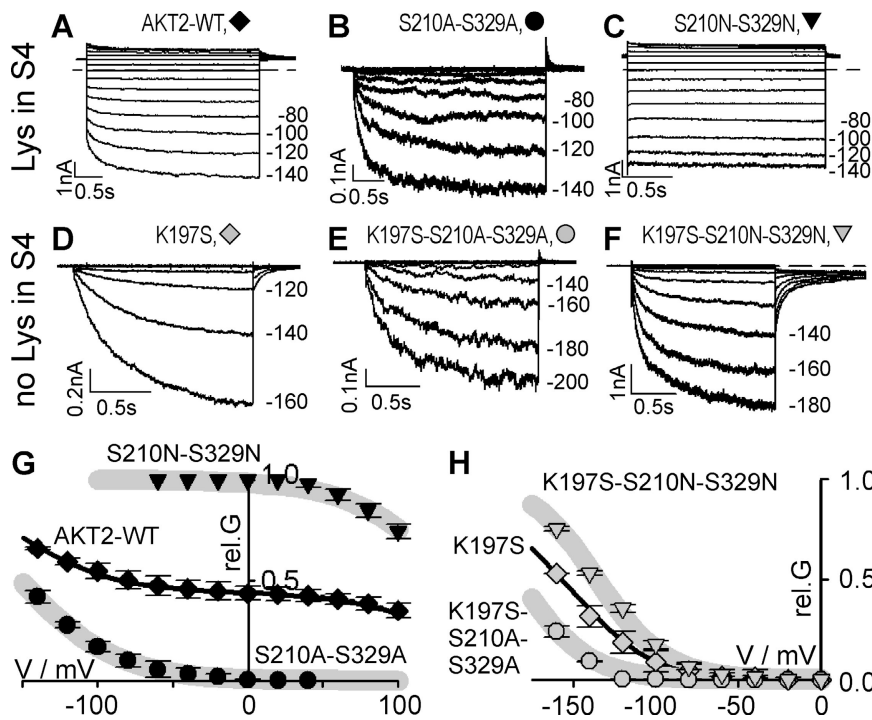
Figure 9. The two different gating modes of the AKT2 wild type and the mutant AKT2-K197S. (A–F) Representative K^+ currents obtained from COS cells expressing AKT2, AKT2-S210A-S329A, AKT2-S210N-S329N, AKT2-K197S, AKT2-K197S-S210A-S329A, and AKT2-K197S-S210N-S329N. Pulse protocols: currents elicited by voltage steps (duration T) from a holding potential of V_H to voltages from V_{min} to V_{max} (20-mV increments) followed by a further voltage step to V_T (pulse protocol indicated as $[V_H; V_{min} ... V_{max}, T; V_T]$ in the following). The dashed lines indicate the zero current level. (A) AKT2; (+40 mV; −140 mV . . . +140 mV, 3 s; +40 mV). (B) The mutant S210A-S329A mimics AKT2-mode#1 gating (+40 mV; −140 mV . . . +40 mV, 3 s; +40 mV). (C) The mutant S210N-S329N mimics AKT2-mode#2 gating (+40 mV; −140 mV . . . +140 mV, 2 s; +40 mV). (D) AKT2-K197S; (0 mV; −160 mV . . . +40 mV, 1.5 s; −80 mV). (E) The mutant K197S-S210A-S329A mimics AKT2-K197S-mode#1 gating (0 mV; −200 mV . . . +40 mV, 1.5 s; 0 mV). (F) The mutant K197S-S210N-S329N mimics AKT2-K197S-mode#2 gating (0 mV; −180 mV . . . +40 mV, 1.5 s; −80 mV). (G) Relative conductance of AKT2 (black diamonds), AKT2-S210A-S329A (black circles), and AKT2-S210N-S329N (black triangles). Data are displayed as mean ± SD (n = 3–6). Gray lines represent nonlinear least-squares fittings of Eq. 4 to the data for S210A-S329A and S210N-S329N ($R^2 > 0.95$). Fits were constrained by the adjustment of a common value δ for both datasets, yielding δ = 0.78, $V_{1/2}^{S210A-S329A}$ = −151.9 mV, $V_{1/2}^{S210N-S329N}$ = +136.0 mV. The solid line represents a weighted sum of the two gray lines: fit_rel.G_{AKT2} = 0.56 × fit_rel.$G_{S210A-S329A}$ + 0.44 × fit_rel.$G_{S210N-S329N}$. (H) Relative conductance of AKT2-K197S (gray diamonds), AKT2-K197S-S210A-S329A (gray circles), and AKT2-K197S-S210N-S329N (gray triangles). Data are displayed as mean ± SD (n = 3–6). Gray lines represent nonlinear least-squares fittings of Eq. 4 to the data for K197S-S210A-S329A and K197S-S210N-S329N ($R^2 > 0.95$). Fits were constrained by the adjustment of a common value δ for both datasets, yielding δ = 1.22, $V_{1/2}^{K197S-S210A-S329A}$ = −183.1 mV, $V_{1/2}^{K197S-S210N-S329N}$ = −135.5 mV. The solid line represents a weighted sum of the two gray lines: fit_rel.G_{K197S} = 0.46 × fit_rel.$G_{K197S-S210A-S329A}$ + 0.54 × fit_rel.$G_{K197S-S210N-S329N}$.

K_{in} channels, like e.g., KAT1. Similar to AKT2-K197S, the effects of phosphorylation on KAT1 channel gating are hardly observable (Tang and Hoshi, 1999). Thus, the presence of the lysine residue K197 in the putative voltage sensor of AKT2 sensitizes the K_{weak} channel to phosphoregulation.

DISCUSSION

The weak rectification of the channel AKT2 is unique among all *Shaker*-like K^+ channels of the model plant *Arabidopsis thaliana*. The ability to mediate both potassium uptake and release is the major characteristic of members of the K_{weak} channel subfamily and suggests that AKT2-like channels have enough functional flexibility to perform different tasks in the plant (Marten et al., 1999; Lacombe et al., 2000; Ache et al., 2001; Deeken et al., 2002). Besides these physiological aspects, the unique gating behavior of AKT2-like channels is also interesting from the biophysical/mechanistic point of view. Previous studies suggested that, despite their unique characteristics, K_{weak} channels share some functional similarities with K_{in} channels (e.g.,

their activation upon hyperpolarization). In this study we generated mutants of the K_{weak} channel AKT2 and created chimeras between AKT2 and the K_{in} channel KAT1 in order to get molecular insights into the mechanistic similarities and differences between K_{weak} and K_{in} channels.

Rectification Properties of K_{weak} Channels Do Not Depend on the Pore Region

The results presented here demonstrate that the weak rectification of AKT2 is not correlated with the structure of the pore, contrasting apparently a previous report by Hoth et al. (2001). Hoth and coworkers exchanged the pore region of the K_{weak} channel AKT3 (=AKT2-M1_D15del; nomenclature according to den Dunnen and Antonarakis, 2001) with that of the plant K_{in} channel KST1 (a channel homologous to KAT1 and 75% identical to KAT1 in the exchanged region). The resulting chimera was characterized as an inward-rectifying channel. The inverse chimera (i.e., KST1 bearing the pore region of AKT2) was characterized as a weak-rectifying channel. From their results, Hoth et al. concluded that essential elements for the rectifica-
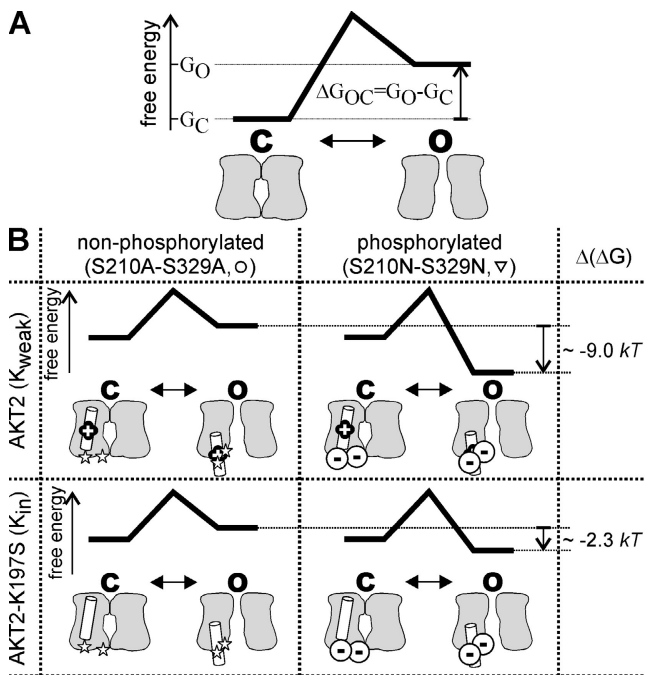
Figure 10. A model to illustrate the sensitization effect of the lysine residue. (A) A channel can exist in two conformations: open, O, and closed, C. The energy difference between open and closed conformation is $\Delta G_{OC} = G_O - G_C$. The probability to find the channel in the open conformation calculates as $p_O = (1 + \exp[\Delta G_{OC}/(kT)])^{-1}$ (Boltzmann function). From the fits to the data in Fig. 9 (G and H), the ΔG_{OC} values for the four channels S210A-S329A, S210N-S329N, K197S-S210A-S329A, and K197S-S210N-S329N are known: $\Delta G_{OC}^{S210A-S329A} = (0.78 \times F/[RT] \times [V + 151.9$ mV$]) \times kT$, $\Delta G_{OC}^{S210N-S329N} = (0.78 \times F/[RT] \times [V - 136.0$ mV$]) \times kT$, $\Delta G_{OC}^{K197S-S210A-S329A} = (1.22 \times F/[RT] \times [V + 183.1$ mV$]) \times kT$, and $\Delta G_{OC}^{K197S-S210N-S329N} = (1.22 \times F/[RT] \times [V + 135.5$ mV$]) \times kT$. (B) Consideration of four different situations: the channel can be phosphorylated (mimicked by the S210N-S329N mutation) or nonphosphorylated (mimicked by the S210A-S329A mutation), and the S4 region of the channel can contain the lysine residue (AKT2, K_{weak}, "+") or not (AKT2-K197S, K_{in}). The effect of channel phosphorylation, i.e., the energy difference, $\Delta(\Delta G) = \Delta G_{OC}^P - \Delta G_{OC}^{non-P}$, between the open conformations of a phosphorylated (mode#2) and a nonphosphorylated (mode#1) channel, can be approximated by calculating the difference in the ΔG_{OC} values between the mutants mimicking the phosphorylated and nonphosphorylated state: $\Delta(\Delta G^{AKT2}) = \Delta G_{OC}^{S210N-S329N} - \Delta G_{OC}^{S210A-S329A} \approx -9.0$ kT, and $\Delta(\Delta G^{K197S}) = \Delta G_{OC}^{K197S-S210N-S329N} - \Delta G_{OC}^{K197S-S210A-S329A} \approx -2.3$ kT. It should be noted that the value obtained for the AKT2 wild type is well in line with the energy difference $\Delta(\Delta G) = \Delta G_{OC}^{mode\#2} - \Delta G_{OC}^{mode\#1} \approx -8.5$ kT obtained from the data in Fig. 6 D.

tion are located within the channel pore (Hoth et al., 2001). The results of our study here do not support this conclusion: on the one hand, when the pore of AKT2 was exchanged with that of the K_{in} channel KAT1, the chimera was still weakly rectifying. On the other hand, the three purely inward-rectifying AKT2 mutants K197S, K197D, and S210A-S329A comprised the AKT2 pore.

Instead, the data here and a series of previous studies (Dreyer et al., 2001; Chérel et al., 2002; Michard et al., 2005) provide growing evidence for an alternative concept: (a) the weak rectification of AKT2 originates from the superimposition of channels gating in two distinct gating modes; (b) in both gating modes AKT2 channels are activated by hyperpolarization; (c) the main difference between channels of the two gating modes are their strongly distinct activation thresholds, so-called mode#2 channels activate >+200 mV more positive than so-called mode#1 channels; (d) the setting of the gating mode depends on the phosphorylation status of the channel; (e) the voltage sensor influences the response to phosphorylation.

Phosphorylation Feeds Back on Channel Gating

In AKT2 two putative phosphorylation sites (highly conserved among K_{weak} channels) have been pinpointed that are involved in setting the gating modes (Michard et al., 2005). One is located in the S4–S5 linker (AKT2-S210) and the other in the S6–COOH terminus linker (AKT2-S329). Interestingly, previous studies on animal depolarization-activated voltage-gated potassium channels and on hyperpolarization-activated cyclic nucleotide–gated pacemaker channels (HCN) identified these regions to be essential for coupling the voltage sensor to the intracellular activation gate (Chen et al., 2001; Lu et al., 2002). For both potassium channel classes (voltage-gated outward and inward rectifiers) it was shown that the S4–S5 linker and the S6–COOH terminus linker interact and modulate channel gating (Tristani-Firouzi et al., 2002; Decher et al., 2004). These reports suggest a conserved role of the S4–S5 and the S6–COOH terminus linkers in channel gating within the large superfamily of voltage-gated potassium channels. In this context the effect of phosphorylation of the two serine residues in AKT2 (S210 and S329) could be understood in terms of structural rearrangements within the S4–S5 and the S6–COOH terminus linkers, which in turn feed back on channel gating by affecting the activation threshold.

A Lysine Residue in S4 Amplifies the Feedback Process

Phosphorylation of the two serine residues in the S4–S5 linker and in the S6–COOH terminus linker of AKT2 shifts the activation threshold of the channel by >+200 mV positive along the voltage axis. Intriguingly, in this study we uncovered that a highly conserved lysine residue in the S4 segment of AKT2 plays an important role in this feedback process. If K197 was replaced by, e.g., a serine, the response to phosphorylation was so small that it could not be resolved by modulating the activity of endogenous kinases and phosphatases in COS cells and *Xenopus* oocytes. Only the mutation of the phos-

phorylation sites S210 and S329 suggested that AKT2-K197S was still modulated by phosphorylation, however, far weaker than the wild type. It can be concluded that the presence of the lysine residue sensitizes AKT2 to the structural rearrangements in the S4–S5 and S6–COOH terminus linkers induced by phosphorylation (or mimicked by mutations).

Reciprocal Effects of the Coupling between the Voltage Sensor and the Phosphorylated Regions

A previous study on AKT2 revealed that phosphorylation is voltage dependent (Michard et al., 2005), suggesting that the neighbored voltage sensor and the S4–S5 and S6–COOH terminus linkers (Lai et al., 2005) reciprocally affect each other. Recent structural analyses of a depolarization-activated potassium channel have revealed that the movement of the voltage sensor induces structural rearrangements in the S4–S5 and S6–COOH terminus linkers (Long et al., 2005b). We propose a similar mechanism also for AKT2. When AKT2 is in the closed state, the phosphorylation sites in the S4–S5 and S6–COOH terminus linkers (S210 and S329) are very likely shielded by other parts of the channel protein and therefore inaccessible to kinases. The movement of the voltage sensor upon hyperpolarization may induce structural rearrangements in the S4–S5 and S6–COOH terminus linkers, which then may lay the residues S210 and S329 bare to cytosolic kinases. Phosphorylation of these serines in turn may change further the structure of the two linkers and expose sites (either the phosphate groups themselves or other charged/polarized residues of the channel polypeptide), which then interact with the voltage sensor and lock the channel in the open state. The results presented in this study indicate that this interaction, i.e., the response to phosphorylation events, was strongly reduced in the AKT2-K197S mutant but not in the G186R mutant and therefore point to the importance of the lysine residue.

The Structure of the Entire Voltage-sensing Module Is Important for K_{weak} Properties

The lysine residue in S4 plays an essential role in determining the sensitivity of AKT2 toward phosphorylation events. However, the generation of a lysine residue in the S4 segment of the K_{in} channel KAT1 at the position equivalent to AKT2-K197 did not induce any significant change in channel gating (Fig. 11). At first glance this result is not surprising since neither the KAT1 wild type nor the KAT1-S179K mutant comprises any phosphorylation site in the S4–S5 or the S6–COOH terminus linker. At closer inspection, however, the comparison between the mutant KAT1-S179K and the chimera displayed in Fig. 3 A indicated that an additional lysine residue in an S4 segment of a K_{in} channel alone is
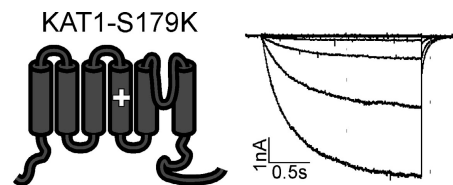
KAT1-S179K

Figure 11. The lysine makes an impact in the AKT2 channel background but not in the KAT1 channel background. The mutant KAT1-S179K is an inward-rectifying K^+ channel. Representative K^+ currents measured in standard solution elicited by voltage steps from a holding potential of 0 mV by 2-s voltage steps to voltages from +60 mV to −180 mV (20-mV decrements) followed by a further voltage step to −80 mV. Data are representative for at least three repeats.

not sufficient to generate a hypersensitive response to changes in the S4–S5 and S6–COOH terminus linkers. The hypersensitive response of the K_{weak} channel AKT2 to phosphorylation therefore depends on the overall structure of the entire voltage-sensing module (segments S1–S4).

Physiological Implications of the Hypersensitive Response to Phosphorylation

Depending on its phosphorylation status an AKT2 channel gates in two distinct gating modes. Actually, current signatures of both AKT2 gating modes have been described in the plant (Bauer et al., 2000; Ivashikina et al., 2005), indicating that the hypersensitive response of K_{weak} channels to phosphorylation is a physiologically relevant mechanism. The bimodal gating behavior renders AKT2-like channels intriguingly versatile. Especially the observation that K_{weak} channel α subunits confer the weak rectification property even to heteromeric K^+ channels (Ache et al., 2001) indicates an important role of the hypersensitive response to phosphorylation at the cellular level. In gating mode#1 (nonphosphorylated) AKT2-like channels act as potassium uptake channels, allowing the cell (driven by plasma membrane H^+-ATPases) to accumulate larger amounts of K^+, e.g., during stomatal opening (Ivashikina et al., 2005). Phosphorylation switches K_{weak} channels from gating mode#1 to gating mode#2 and locks the channel open. This switch not only biases the membrane potential strongly to the equilibrium potential of K^+ and thus stabilizes the membrane voltage (Deeken et al., 2002), it also activates a physiologically important "potassium battery." In fact, "open leak" K^+ channels allow the use of the transmembrane potassium gradient (in addition to the transmembrane proton gradient) to energetically charge other electrogenic transport processes. Thus, by regulating the phosphorylation status of AKT2-like K^+ channel subunits the cell can control whether it charges the potassium battery or whether it makes use of it.

Conclusion

Together with a series of previous studies (Dreyer et al., 2001; Chérel et al., 2002; Michard et al., 2005) the data presented here allow us to reasonably explain the gating characteristics of K_{weak} channels. (a) Weakly rectifying plant K^+ channels (K_{weak} channels) are in fact specialized inwardly rectifying channels (K_{in} channels) in the sense that they activate upon hyperpolarization rather than upon depolarization. (b) The specialization of K_{weak} channels is their hypersensitive response to certain phosphorylation events that shift the activation threshold of the channels by $>+200$ mV positive along the voltage axis. (c) A lysine residue that is highly conserved among K_{weak} channels is essential for this hypersensitive response. Elimination of this lysine residue yielded channel mutants that gated like conventional K_{in} channels (e.g., AKT2-K197S, AKT2-K197D). (d) The lysine residue must be embedded in a proper structure of the voltage-sensing module to make an impact.

The understanding of the gating features of AKT2 suggests that this channel is very likely part (or target) of intra- and intercellular signaling cascades. Consequently, the future challenge will be to comprehend the integration of AKT2-like channels in these (currently unknown) signaling cascades.

REFERENCES

Ache, P., D. Becker, R. Deeken, I. Dreyer, H. Weber, J. Fromm, and R. Hedrich. 2001. VFK1, a *Vicia faba* K$^+$ channel involved in phloem unloading. *Plant J.* 27:571–580.

Amtmann, A., P. Armengaud, and V. Volkov. 2004. Potassium nutrition and salt stress. *In* Membrane Transport in Plants. M.R. Blatt, editor. Blackwell, Oxford. 316–348.

Bauer, C.S., S. Hoth, K. Haga, K. Philippar, N. Aoki, and R. Hedrich. 2000. Differential expression and regulation of K$^+$ channels in the maize coleoptile: molecular and biophysical analysis of cells isolated from cortex and vasculature. *Plant J.* 24:139–145.

Becker, D., I. Dreyer, S. Hoth, J.D. Reid, H. Busch, M. Lehnen, K. Palme, and R. Hedrich. 1996. Changes in voltage activation, Cs$^+$ sensitivity, and ion permeability in H5 mutants of the plant K$^+$ channel KAT1. *Proc. Natl. Acad. Sci. USA.* 93:8123–8128.

Berkowitz, G., X. Zhang, R. Mercie, Q. Leng, and M. Lawton. 2000. Co-expression of calcium-dependent protein kinase with the inward rectified guard cell K$^+$ channel KAT1 alters current parameters in *Xenopus laevis* oocytes. *Plant Cell Physiol.* 41:785–790.

Bezanilla, F. 2000. The voltage sensor in voltage-dependent ion channels. *Physiol. Rev.* 80:555–592.

Bezanilla, F., and E. Perozo. 2003. The voltage sensor and the gate in ion channels. *Adv. Protein Chem.* 63:211–241.

Blatt, M.R. 2004. Membrane Transport in Plants. Blackwell Publishing, Oxford, UK. 372 pp.

Cao, Y., N.M. Crawford, and J.I. Schroeder. 1995a. Amino terminus and the first four membrane-spanning segments of the *Arabidopsis* K$^+$ channel KAT1 confer inward-rectification property of plant-animal chimeric channels. *J. Biol. Chem.* 270:17697–17701.

Cao, Y., J.M. Ward, W.B. Kelly, A.M. Ichida, R.F. Gaber, J.A. Anderson, N. Uozumi, J.I. Schroeder, and N.M. Crawford. 1995b. Multiple genes, tissue specificity, and expression-dependent modulation contribute to the functional diversity of potassium channels in *Arabidopsis thaliana. Plant Physiol.* 109:1093–1106.

Chen, J., J.S. Mitcheson, M. Tristani-Firouzi, M. Lin, and M.C. Sanguinetti. 2001. The S4-S5 linker couples voltage sensing and activation of pacemaker channels. *Proc. Natl. Acad. Sci. USA.* 98: 11277–11282.

Chérel, I., E. Michard, N. Platet, K. Mouline, C. Alcon, H. Sentenac, and J.B. Thibaud. 2002. Physical and functional interaction of the *Arabidopsis* K$^+$ channel AKT2 and phosphatase AtPP2CA. *Plant Cell.* 14:1133–1146.

Decher, N., J. Chen, and M.C. Sanguinetti. 2004. Voltage-dependent gating of hyperpolarization-activated, cyclic nucleotide-gated pacemaker channels—molecular coupling between the S4–S5 and c-Linkers. *J. Biol. Chem.* 279:13859–13865.

Deeken, R., D. Geiger, J. Fromm, O. Koroleva, P. Ache, R. Langenfeld-Heyser, N. Sauer, S.T. May, and R. Hedrich. 2002. Loss of the AKT2/3 potassium channel affects sugar loading into the phloem of *Arabidopsis. Planta.* 216:334–344.

den Dunnen, J.T., and S.E. Antonarakis. 2001. Nomenclature for the description of human sequence variations. *Hum. Genet.* 109: 121–124.

Dreyer, I., S. Antunes, T. Hoshi, B. Mueller-Roeber, K. Palme, O. Pongs, B. Reintanz, and R. Hedrich. 1997. Plant K$^+$ channel α-subunits assemble indiscriminately. *Biophys. J.* 72:2143–2150.

Dreyer, I., D. Becker, M. Bregante, F. Gambale, M. Lehnen, K. Palme, and R. Hedrich. 1998. Single mutations strongly alter the K$^+$-selective pore of the K_{in} channel KAT1. *FEBS Lett.* 430:370–376.

Dreyer, I., C. Horeau, G. Lemaillet, S. Zimmermann, D.R. Bush, A. Rodriguez-Navarro, D.P. Schachtman, E.P. Spalding, H. Sentenac, and R.F. Gaber. 1999. Identification and characterization of plant transporters using heterologous expression systems. *J. Exp. Bot.* 50:1073–1087.

Dreyer, I., E. Michard, B. Lacombe, and J.B. Thibaud. 2001. A plant Shaker-like K$^+$ channel switches between two distinct gating modes resulting in either inward-rectifying or "leak" current. *FEBS Lett.* 505:233–239.

Dreyer, I., B. Mueller-Roeber, and B. Köhler. 2004. Voltage-gated ion channels. *In* Membrane Transport in Plants. M.R. Blatt, editor. Blackwell Publishing, Oxford. 150–192.

Geiger, D., D. Becker, B. Lacombe, and R. Hedrich. 2002. Outer pore residues control the H$^+$ and K$^+$ sensitivity of the *Arabidopsis* potassium channel AKT3. *Plant Cell.* 14:1859–1868.

Hedrich, R., O. Moran, F. Conti, H. Busch, D. Becker, F. Gambale, I. Dreyer, A. Kuch, K. Neuwinger, and K. Palme. 1995. Inward rectifier potassium channels in plants differ from their animal counterparts in response to voltage and channel modulators. *Eur. Biophys. J.* 24:107–115.

Hoshi, T. 1995. Regulation of voltage dependence of the KAT1 channel by intracellular factors. *J. Gen. Physiol.* 105:309–328.

Hoth, S., I. Dreyer, P. Dietrich, D. Becker, B. Mueller-Roeber, and R. Hedrich. 1997. Molecular basis of plant-specific acid activation of K$^+$ uptake channels. *Proc. Natl. Acad. Sci. USA.* 94:4806–4810.

Hoth, S., D. Geiger, D. Becker, and R. Hedrich. 2001. The pore of

plant K^{+} channels is involved in voltage and pH sensing: domain-swapping between different K^{+} channel α-subunits. *Plant Cell.* 13: 943–952.

Ivashikina, N., R. Deeken, S. Fischer, P. Ache, and R. Hedrich. 2005. AKT2/3 subunits render guard cell K^{+} channels Ca^{2+} sensitive. *J. Gen. Physiol.* 125:483–492.

Ketchum, K.A., and C.W. Slayman. 1996. Isolation of an ion channel gene from *Arabidopsis thaliana* using the H5 signature sequence from voltage-dependent K^{+} channels. *FEBS Lett.* 378:19–26.

Lacombe, B., G. Pilot, E. Michard, F. Gaymard, H. Sentenac, and J.B. Thibaud. 2000. A shaker-like K^{+} channel with weak rectification is expressed in both source and sink phloem tissues of *Arabidopsis. Plant Cell.* 12:837–851.

Lai, H.C., M. Grabe, Y.N. Jan, and L.Y. Jan. 2005. The S4 voltage sensor packs against the pore domain in the KAT1 voltage-gated potassium channel. *Neuron.* 47:395–406.

Latorre, R., R. Olcese, C. Basso, C. Gonzalez, F. Munoz, D. Cosmelli, and O. Alvarez. 2003. Molecular coupling between voltage sensor and pore opening in the *Arabidopsis* inward rectifier K^{+} channel KAT1. *J. Gen. Physiol.* 122:459–469.

Li, J., Y.R. Lee, and S.M. Assmann. 1998. Guard cells possess a calcium-dependent protein kinase that phosphorylates the KAT1 potassium channel. *Plant Physiol.* 116:785–795.

Long, S.B., E.B. Campbell, and R. MacKinnon. 2005a. Crystal structure of a mammalian voltage-dependent *Shaker* family K^{+}-channel. *Science.* 309:897–903.

Long, S.B., E.B. Campbell, and R. MacKinnon. 2005b. Voltage sensor of Kv1.2: structural basis of electromechanical coupling. *Science.* 309:903–908.

Lu, Z., A.M. Klem, and Y. Ramu. 2002. Coupling between voltage sensors and activation gate in voltage-gated K^{+} channels. *J. Gen. Physiol.* 120:663–676.

MacKinnon, R. 1991. Determination of the subunit stoichiometry of a voltage-activated potassium channel. *Nature.* 350:232–235.

Männikkö, R., F. Elinder, and H.P. Larsson. 2002. Voltage-sensing mechanism is conserved among ion channels gated by opposite voltages. *Nature.* 419:837–841.

Marquardt, D.W. 1963. An algorithm for least squares estimation of nonlinear parameters. *J. Soc. Ind. Appl. Math.* 11:431–441.

Marten, I., S. Hoth, R. Deeken, P. Ache, K.A. Ketchum, T. Hoshi, and R. Hedrich. 1999. AKT3, a phloem-localized K^{+} channel, is blocked by protons. *Proc. Natl. Acad. Sci. USA.* 96:7581–7586.

Michard, E., I. Dreyer, B. Lacombe, H. Sentenac, and J.B. Thibaud. 2005. Inward rectification of the AKT2 channel abolished by voltage-dependent phosphorylation. *Plant J.* 10.1111/j.1365-313X.2005.02566.x

Mori, I.C., N. Uozumi, and S. Muto. 2000. Phosphorylation of the inward-rectifying potassium channel KAT1 by ABR kinase in *Vicia* guard cells. *Plant Cell Physiol.* 41:850–856.

Mueller-Roeber, B., J. Ellenberg, N. Provart, L. Willmitzer, H. Busch, D. Becker, P. Dietrich, S. Hoth, and R. Hedrich. 1995. Cloning and electrophysiological analysis of KST1, an inward rectifying K^{+} channel expressed in potato guard cells. *EMBO J.* 14: 2409–2416.

Pilot, G., R. Pratelli, F. Gaymard, Y. Meyer, and H. Sentenac. 2003. Five-group distribution of the Shaker-like K^{+} channel family in higher plants. *J. Mol. Evol.* 56:418–434.

Sakmann, B., and E. Neher, editors. 1995. Single-Channel Recording. Second edition. Plenum Press, New York. 700 pp.

Swartz, K.J. 2004. Towards a structural view of gating in potassium channels. *Nat. Rev. Neurosci.* 5:905–916.

Tang, X.D., and T. Hoshi. 1999. Rundown of the hyperpolarization-activated KAT1 channel involves slowing of the opening transitions regulated by phosphorylation. *Biophys. J.* 76:3089–3098.

Tristani-Firouzi, M., J. Chen, and M.C. Sanguinetti. 2002. Interactions between S4-S5 linker and S6 transmembrane domain modulate gating of HERG K^{+} channels. *J. Biol. Chem.* 277:18994–19000.

Véry, A.A., F. Gaymard, C. Bosseux, H. Sentenac, and J.B. Thibaud. 1995. Expression of a cloned plant K^{+} channel in *Xenopus* oocytes: analysis of macroscopic currents. *Plant J.* 7:321–332.

Véry, A.A., and H. Sentenac. 2003. Molecular mechanisms and regulation of K^{+} transport in higher plants. *Annu. Rev. Plant Biol.* 54: 575–603.

Yellen, G. 2002. The voltage-gated potassium channels and their relatives. *Nature.* 419:35–42.

Zei, P.C., and R.W. Aldrich. 1998. Voltage-dependent gating of single wild-type and S4 mutant KAT1 inward rectifier potassium channels. *J. Gen. Physiol.* 112:679–713.